© 2025 Journal of Pharmacy & Pharmacognosy Research, 13 (4), 1191-1201, 2025
ISSN 0719-4250
https://jppres.com

DOI: https://doi.org/10.56499/jppres24.2231_13.4.1191

Original Article

Pharmacognostic analysis and teachable machine automated identification of *Uvae ursi folium*, *Vitis idaeae folium* and *Buxi folium*

[Análisis farmacognóstico e identificación automatizada con máquina enseñable de *Uvae ursi folium*, *Vitis idaeae folium* y *Buxi folium*]

Asen N. Stoyanov*, Trayan M. Gruykin, Miroslav Y. Boyadzhiev, Ventsislav V. Popovski

Department of Organic Chemistry and Pharmacognosy, Sofia University "St. Kliment Ohridski", Sofia, 15 Tsar Osvoboditel Blvd, Bulgaria.
*E-mail: asenns@uni-sofia.bg

Abstract

Context: Microscopic analysis is a method in Pharmacognosy utilized in identifying herbal substances. Machine learning and computer vision are contemporary approaches leveraged in the identification of plants. Bearberry leaf is an active ingredient of medicinal products used to treat mild infections of the lower urinary tract. In the present study, we examine the unique microscopic diagnostic characteristics of *Uvae ursi folium* and two of its adulterants - *Vitis idaeae folium* and *Buxi folium* and evaluate the effectiveness of teachable machine models in automated microscopic preparation identification.

Aims: To examine *Uvae ursi folium*, *Vitis idaeae folium* and *Buxi folium* micromorphology and micrometry and evaluate the effectiveness of teachable machine models in their microscopic identification.

Methods: Microscopic preparations were mounted in 4 g/mL chloral hydrate aqueous solution. Photographic materials were captured using a Zeiss Primostar iLED microscope and analyzed in Labscope 4.2.1. Models were trained on datasets of photographic materials, compared by their intrinsic parameters (accuracy per class, confusion matrix, accuracy per epoch, and loss per epoch), and tested on datasets of 10 unseen images.

Results: Microscopic descriptions, illustrations, and photographic materials were created for all herbal substances. *Vitis idaeae folium* and *Buxi folium* covering and glandular trichomes were described. Teachable machine models successfully distinguish between and identify the herbal substances. The most accurate models correctly identify all tested *Uvae ursi folium* photographic materials.

Conclusions: *Vitis idaeae folium* and *Buxi folium* diagnostic characteristics are described, and teachable machine model capabilities in automated microscopic photographic material identification are explored for the first time.

Keywords: *Arctostaphylos uva-ursi*; *Buxus sempervirens*; computer vision; machine learning; microscopy; *Vaccinium vitis-idaea*.

Resumen

Contexto: El análisis microscópico es un método en farmacognosia utilizado para la identificación de sustancias herbales. El aprendizaje automático y la visión por computadora son enfoques contemporáneos empleados en la identificación de plantas. La hoja de gayuba es un ingrediente activo de productos medicinales utilizados para tratar infecciones leves del tracto urinario inferior. En el presente estudio, examinamos las características diagnósticas microscópicas únicas de *Uvae ursi folium* y dos de sus adulterantes - *Vitis idaeae folium y Buxi folium* - y evaluamos la efectividad de los modelos de *teachable machine* en la identificación automatizada de preparaciones microscópicas.

Objetivos: Examinar la micromorfología y micrometría de *Uvae ursi folium*, *Vitis idaeae folium* y *Buxi folium*, y evaluar la efectividad de los modelos de *teachable machine* en su identificación microscópica.

Métodos: Las preparaciones microscópicas se montaron en una solución acuosa de hidrato de cloral de 4 g/mL. Se capturaron materiales fotográficos utilizando un microscopio Zeiss Primostar iLED y se analizaron en Labscope 4.2.1. Los modelos fueron entrenados con conjuntos de datos de materiales fotográficos, comparados según sus parámetros intrínsecos (precisión por clase, matriz de confusión, precisión por época, pérdida por época) y probados con conjuntos de datos de 10 imágenes no vistas.

Resultados: Se crearon descripciones microscópicas, ilustraciones y materiales fotográficos para todas las sustancias herbales. Se describieron los tricomas de cobertura y glandulares de *Vitis idaeae folium* y *Buxi folium*. Los modelos de *teachable machine* distinguen e identifican exitosamente las sustancias herbales. Los modelos más precisos identifican correctamente todos los materiales fotográficos de *Uvae ursi folium* probados.

Conclusiones: Se describen las características diagnósticas de *Vitis idaeae folium* y *Buxi folium*, y se exploran por primera vez las capacidades de los modelos de *teachable machine* en la identificación automatizada de materiales fotográficos microscópicos.

Palabras Clave: aprendizaje automático; *Arctostaphylos uva-ursi*; *Buxus sempervirens*; microscopía; *Vaccinium vitis-idaea*; visión por computadora.

ARTICLE INFO
Received: September 19, 2024.
Accepted: February 25, 2025.
Available Online: April 24, 2025.

AUTHOR INFO
ORCID:
0009-0005-1957-9731 (ANS)
0009-0002-4818-5780 (TMG)
0009-0005-8425-6402 (MYB)
0009-0006-6836-8284 (VVP)

INTRODUCTION

Bearberry, *Arctostaphylos uva-ursi* (L.) Spreng. (*Ericaceae*), is a well-known medicinal plant in systems of traditional herbal medicine, used for the symptomatic treatment of lower urinary tract complaints, namely mild, uncomplicated infections (Bokelmann, 2022; Nedelcheva and Draganov, 2014). The morphological part of primary interest is the dried, whole, or fragmented leaf of the plant (*Uvae ursi folium*), due in part to its bioaccumulation of simple phenol glycosides like arbutin and methyl arbutin (Migas and Krauze-Baranowska, 2015) and antimicrobial activity (Cybulska et al., 2011). An analysis of patient attitudes shows that over half (52.2%) of the respondents use herbal products in the treatment of urinary tract infections, the majority of which (52.1%) contain *Uvae ursi folium* (Jovanović et al., 2024). Known common adulterants of the herbal substance are the leaves of lingonberry, *Vaccinium vitis-idaea* L. (*Ericaceae*) - *Vitis idaeae folium*, and the leaves of box, *Buxus sempervirens* L. (*Buxaceae*) - *Buxi folium*. They are included in *Uvae ursi folium* samples either accidentally or on purpose due to their macroscopic morphological resemblance (Radulović et al., 2010). The risk of accidental bearberry adulteration with lingonberry leaves during collection is further increased due to the same distribution and habitus of the species (Assyov and Petrova, 2012; Radulović et al., 2010). While the macroscopic characteristics of *Uvae ursi folium*, *Vitis idaeae folium*, and *Buxi folium* are well described, few micromorphological studies have been carried out on the adulterant herbal substances (Gostin, 2009), and none with the goal of determining diagnostic characteristics of the adulterant herbal substances. Consequently, a comparative analysis of diagnostic fragments of the three herbal substances has also not been carried out. Some studies explore leaf micromorphology during pathology (Guo et al., 2020), but little emphasis is placed on leaf structures other than stomata. So far, pharmacognostic microscopic analysis has not been carried out and published on bearberry leaf adulterants in bright-field. While human vision is superior in 3D object recognition (Welchman, 2016), the untrained eye can easily confuse plants even under close examination (Cornara et al., 2018). Considering the lack of scientific literature on *Uvae ursi folium* adulterant micromorphology, we deem it prudent to explore the capabilities of machine learning-aided identification of the herbal substances in addition to describing their diagnostic microscopic characteristics.

Machine learning and computer vision are contemporary approaches with broad areas of application, leveraged in multiple fields of study in the process of automated image recognition. Those relating to Pharmacognosy, Pharmaceutical Botany and Plant Sciences include but are not limited to the identification and classification of medicinal and poisonous plants (Azadnia et al., 2024; Kavitha et. al., 2023; Oppong et al., 2022) and herbarium specimens (Hussein et al., 2022) and identification and classification of plant pathologies (Choudhary et al., 2023). Various such instruments have been created and evaluated. One such web-based, low-barrier-of-entry tool that requires no specialized technical expertise or extensive programming knowledge is Google's teachable machine (Carney et al., 2020). Although it was initially created to aid in educating the public in machine learning, it has since posed interest for researchers in various fields, specifically due to its flexibility and approachability. Teachable machines have been utilized in animal species classification (Wong and Fadzly, 2022), forest fire detection (Grari et al., 2024), dental caries detection (Anh et al., 2024), and leaf classification (Parate et al., 2023), among others. Attempts have also been made to optimize teachable machine plant image recognition (Malahina et al., 2024).

Despite the rising interest in computer vision and machine learning, the capabilities of such models in determining the microscopic identity of herbal substance samples in Pharmacognosy remain largely unexplored. Furthermore, scientific literature lacks comprehensive information on the micromorphology of *Uvae ursi folium* adulterants, which warrants further investigations in this area. In this context, we outline the primary objectives of the study. First, we characterized *Vitis idaeae folium* and *Buxi folium* micromorphology and micrometry in bright-field and compared them with *Uvae ursi folium* micromorphology and micrometry to highlight unique herbal substance diagnostic characteristics. Second, we developed and evaluated machine learning models in teachable machines, which attempt to distinguish between *Uvae ursi folium* and adulterant herbal substances based on these microscopic diagnostic characteristics.

MATERIAL AND METHODS

Herbal substance acquisition

Leaves from *Arctostaphylos uva-ursi* (L.) Spreng. (*Ericaceae*) and *Vaccinium vitis-idaea* L. (*Ericaceae*) were obtained in July 2022 from the Razlozhki Suhodol area in Northern Pirin, Bulgaria (GPS coordinates: 41.839884, 23.390609). Plant identification on site was carried out by Prof. Anely Nedelcheva of the Department of Organic Chemistry and Pharmacognosy at Sofia University "St. Kliement Ohridski". *Buxus sem-*

pervirens L. (*Buxaceae*) leaves were collected from the botanical gardens of Sofia University "St. Kliment Ohridski". Collection and primary processing were achieved by cutting off fresh branches of the plants, which were then subjected to horizontal drying at normal conditions away from direct sunlight. The leaves were then removed by hand. The dried herbal substances were analyzed macroscopically for other morphological parts from the same or different plants. Any foreign matter and damaged or discolored leaves were removed. Voucher materials were deposited in the Laboratory of Pharmacognosy voucher material collection at Sofia University "St. Kliment Ohridski" under the codenames UUF222401, VIF222401, and BUF222401.

Microscopic examination

Each herbal substance was reduced to a fine powder with a mortar and pestle. A 4 g/mL chloral hydrate (Honeywell, 99.5%) aqueous solution was used as a mounting and clearing agent. The powder for examination was dispersed in 2-3 drops of mounting solution on a glass slide, a cover slip was placed, and the preparation was then boiled over an alcohol burner until sufficient discoloration was achieved. Photographic materials were taken with a Zeiss Primostar iLED compound microscope and then analyzed with Zeiss Labscope 4.3.1 software. Scaling calibration was performed manually. Leaf micromorphology and relevant linear measurements and micrometry were then determined and compared. Diagnostic fragments of note described were the cuticle surface, epidermis pavement cell shape, stomata type, covering and glandular trichome presence and type, and presence of fibers and crystals. Cuticle width, abaxial and adaxial epidermis pavement cell perimeter and area, and the length of the first layer of palisade parenchyma cells in transverse view were measured, and the stomatal index was calculated using a standard equation [1] (Mukherjee, 2019).

$$SI = (S \times 100) / (E + S) \quad [1]$$

Where S is the number of stomata in a given area of leaf, E is the number of epidermal (pavement) cells in the same area, and SI is the stomatal index in percentage (%).

Figures of each herbal substance's diagnostic characteristics were prepared by hand-drawing over an overlay of the photographic materials in Procreate, Savage Interactive Pty Ltd. Individual fragment illustrations were then compounded to create micromorphological illustrations incorporating all drawn tissue fragments in Adobe Photoshop 2024, Adobe Inc. Care was taken to retain the original size and proportions of each fragment in the process of composing the compounded illustrations.

Statistical analysis

Data obtained from measuring the herbal substance's microscopic diagnostic characteristics are expressed as the mean ± standard error of the mean (SEM). At least 50 measurements were made. One-way ANOVA and Tukey statistical analyses were performed using Microsoft Excel (2024), Microsoft Corporation. The values obtained at significance levels of $p \leq 0.05$ were considered statistically significant.

Machine learning model development

Machine learning models were developed using Google Teachable Machine 2.0 – image classification project type, standard image mode. The models were trained using datasets composed of 32-bit microscopic photographic materials of key diagnostic fragments from each herbal substance. The photographic materials were categorized based on the depicted diagnostic characteristics. Categories selected for algorithm training were abaxial epidermis in surface view bearing stomata, adaxial epidermis in surface view, adaxial epidermis in transverse view, and spongy parenchyma. This selection was contingent on our observations during microscopic examination. Each image was cropped to a standardized size of 5 cm x 5 cm at a resolution of 300 dpi (dots per inch), ensuring the photographic materials focused exclusively on the relevant diagnostic fragment. A total of 50 images were collected for each diagnostic characteristic, resulting in 200 photographic materials per herbal substance (50 images per diagnostic fragment).

To further structure the training dataset, image collages of diagnostic features were created for each herbal substance. The collage canvas size was 10 cm × 10 cm at a resolution of 300 dpi. Each collage contained four images, one from each diagnostic category (adaxial epidermis in surface and transverse views, stomata, and spongy parenchyma). The placement of these images within the collage was standardized to maintain a consistent arrangement across all collages. A total of 50 collages were created for each herbal substance, resulting in a dataset of 150 collages.

During the training process, we explored the model performance at 10, 25, and 50 epochs and maintained a constant batch size of 16 and a learning rate of 0.001 and recorded the intrinsic model parameters – accuracy per class, accuracy, test accuracy, loss, and test loss. Following training, model classification performance was evaluated by testing with 10 new, unseen photographic materials and collages of the same diagnostic fragments that were not included in the training dataset. Successful identification was defined as the model correctly classifying the unseen photographic material (attributing the highest confidence

level to the correct herbal substance) with at least 20% higher confidence than the second highest classification. For example, when testing with *Uvae ursi folium* photographic material, a confidence level of 4% for *Buxi folium*, 94% for *Uvae ursi folium*, and 2% for *Vitis idaeae folium* would be deemed a successful identification. If the difference between the two highest confidence levels was less than 20%, but the highest was attributed to the correct herbal substance (for example when testing for *Uvae ursi folium* we obtain a confidence level of 42% for *Buxi folium*, 55% for *Uvae ursi folium* and 3% for *Vitis idaeae folium*) this would be deemed a semi-successful identification. Incorrectly classifying the fragment (the highest confidence level being assigned to the wrong herbal substance) would be considered an unsuccessful identification.

Machine learning model evaluation metrics

Quantifying model performance after training should be based on appropriate evaluation metrics for qualitative methods, such as machine learning assisted microscopic identification of powdered herbal substances. This assessment requires the use of informed metrics such as accuracy, precision, sensitivity, and F1 score (Powders, 2011). For their calculation we define the following measures – TP (true positive): successful identification of *Uvae ursi folium*; 0.5*TP is a semi-succesful identification of *Uvae ursi folium*; TN (true negative): the sum of successful identifications of *Buxi folium* and *Vitis idaeae folium*; FP (false positive): unsuccessful identifications of *Buxi folium* and *Vitis idaeae folium*, confused with *Uvae ursi folium*; FN (false negative): unsuccessful identifications of *Uvae ursi folium*.

Accuracy quantified correctly identified herbal substances by mean equation [2]. The accuracy quantified thusly is a common assessment metric and was different than the accuracy reported by the machine learning models during training.

$$\text{Accuracy} = (TP + 0.5 \times TP + TN) / (TP + 0.5 \times TP + FP + FN) \quad [2]$$

Precision evaluated the models' accuracy in identifying *Uvae ursi folium* correctly according to the equation [3]. Models with a high precision score correctly identified the majority of bearberry leaf microscopic test dataset images, while those with lower scores misidentified adulterant herbal substances as *Uvae ursi folium*.

$$\text{Precision} = TP / (TP + 0.5 \times TP + FP) \quad [3]$$

High sensitivity also showed model accuracy in identifying *Uvae ursi folium* by means of equation [4]. However, models with low sensitivity misidentified *Uvae ursi folium* as an adulterant herbal substance.

$$\text{Sensitivity} = TP / (TP + 0.5 \times TP + FN) \quad [4]$$

The calculation of the F1 score factors in both model precision and sensitivity was defined as the harmonic mean of the two-evaluation metrics by the equation [5].

$$F1 = (2 \times \text{Precision} \times \text{Sensitivity}) / (\text{Precision} + \text{Sensitivity}) \quad [4]$$

The robustness of this qualitative method is determined by the quality of the constructed microscopic image training datasets. As such, images captured with different microscopic techniques or lower-quality microphotography cameras may not be properly identified. The working range of the models is restricted to the herbal substances considered during their creation and included in training datasets. For example, a microscopic image of abaxial epidermis bearing stomata from other herbal substances will always be either a false positive or a false negative identification.

RESULTS

Herbal substance micromorphology

The micromorphological studies of *Uvae ursi folium* and its adulterants show several similarities. The powders of the three herbal substances ranged from greenish grey to yellowish green. All three microscopic preparations were comprised of tissue fragments typical of bifacial leaves. Most notable qualitative differences were observed in pavement cell shape and cell wall structure, stomata type, presence and type of trichomes, and presence of oil globules. Descriptions of each herbal substance's micromorphological diagnostic characteristics are provided and later compared in Table 1. Photographic materials of diagnostic characteristics are compared in Fig. 1.

The microscopic preparations made from powdered *Vaccinium vitis-idaea* L. leaf show fragments of the adaxial epidermis in surface view, showing a distinctly striated cuticle, underlying irregularly polygonal pavement cells with slightly curved and beaded cell walls, and palisade parenchyma. Fragments of abaxial parenchyma in surface view, showing irregularly polygonal pavement cells with somewhat curved and beaded cell walls, non-discreet anisocytic and paracytic stomata, and trichome scars, often accompanied by fragments of spongious parenchyma, with notably large extracellular spaces, positioned underneath the stomata. Parenchymatous cells have beaded walls that are less pronounced compared with pavement cell walls. Fragments of the vascular system show pitted vessels accompanied by rectangular to ovate cells and fibers with pitted cell walls. Fragments of curved, unicellular covering trichomes with

a narrow lumen and warty cuticle. Fragments of brown, multicellular, clavate glandular trichomes, frequently bi- to triseriate at the base. *Vitis idaeae folium* diagnostic fragments are depicted in Fig. 2.

Table 1. Comparison of micromorphological diagnostic characteristic descriptions of *Uvae ursi folium*, *Vitis idaeae folium*, *Buxi folium*.

Microscopic diagnostic characteristics	**Herbal substances**		
	Uvae ursi folium	***Vitis idaeae folium***	***Buxi folium***
Cuticle in surface view	Uniform	Striated	Uniform
Pavement cell shape	Irregular polygon	Irregular polygon	Mostly pentagonal or hexagonal
Pavement cell wall shape	Curved, beaded	Curved, beaded	Straight, rarely beaded
Stomata type	Anomocytic, discreet	Anisocytic and paracytic	Anomocytic, raised
Spongious parenchyma cell wall shape	Beaded	Beaded	Straight, rarely beaded
Covering trichomes	Unicellular, slightly curved	Unicellular, curved	Multicellular, uniseriate
Glandular trichomes	Absent	Multicellular, clavate	Absent
Oil globules	Rare	Rare	Abundant

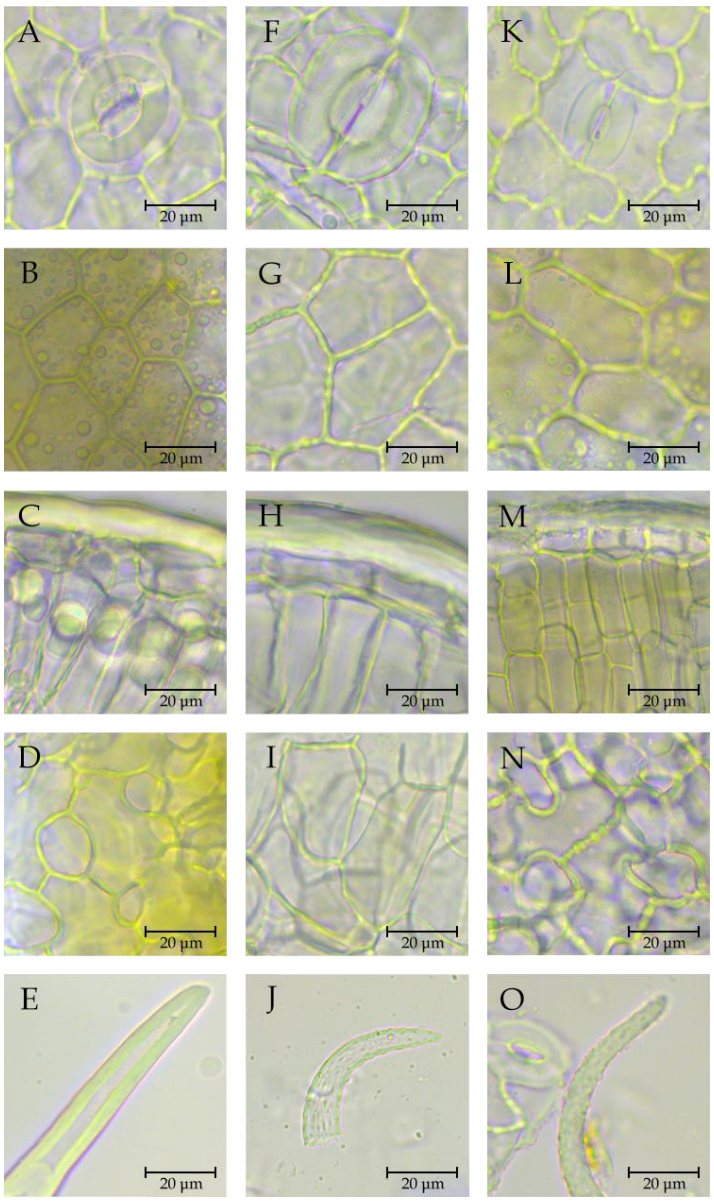

Figure 1. Comparison of micromorphological diagnostic characteristic photographic materials of herbal substances.

Buxi folium **(A)** abaxial epidermis bearing stomata; **(B)** adaxial epidermis in surface view; **(C)** adaxial epidermis in transverse view; **(D)** spongious parenchyma; **(E)** fragment of covering trichome; *Uvae ursi folium* **(F)** abaxial epidermis bearing stomata; **(G)** adaxial epidermis in surface view; **(H)** adaxial epidermis in transverse view; **(I)** spongious parenchyma; **(J)** fragment of covering trichome; *Vitis idaeae folium* **(K)** abaxial epidermis bearing stomata; **(L)** adaxial epidermis in surface view; **(M)** adaxial epidermis in transverse view; **(N)** spongious parenchyma; and **(O)** fragment of covering trichome. Camera Zeiss Primostar iLED, magnification 400×.

.

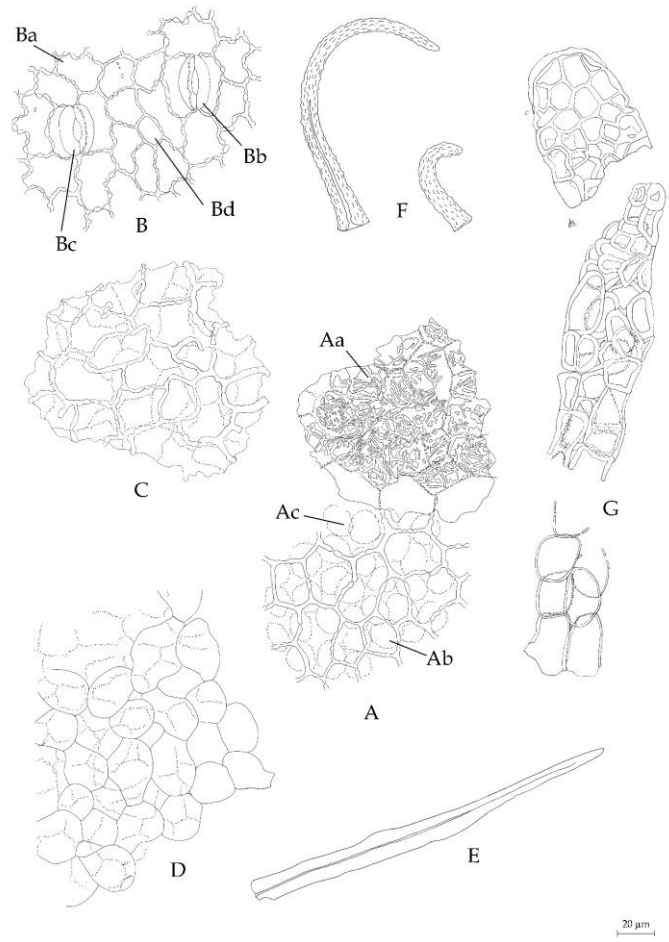

Figure 2. Micromorphological diagnostic characteristics of Lingonberry leaf (*Vitis idaeae folium*) in bright field, 400x magnification.

Fragments of adaxial parenchyma in surface view **(A)**, striated cuticle **(Aa)**, pavement cells **(Ab)** and palisade parenchyma **(Ac)**. Fragments of abaxial parenchyma in surface view **(B)**, showing pavement cells **(Ba)**, paracytic stomata **(Bb)**, anisocytic stomata **(Bc)** and trichome scars **(Bd)**. Fragments of spongious parenchyma in dorsal view **(C)** and transverse view **(D)**. Fragments of fibers **(E)**. Fragments of curved covering trichomes **(F)** and multicellular glandular trichomes **(G)**. Author: Asen Stoyanov.

The microscopic preparations made from powdered *Buxus sempervirens* L. leaf show fragments of adaxial epidermis in surface view, showing straight-walled, mostly pentagonal and hexagonal pavement cells and underlying palisade parenchyma, often containing multiple spherical oil globules. Fragments of abaxial epidermis in surface view, showing straight-walled, mostly pentagonal and hexagonal pavement cells, with underlying spongious parenchyma sometimes containing spherical oil globules. Additionally, slightly raised anomocytic stomata are also observable. Guard cells are covered and encircled by a cuticular thickening. Fragments of the vascular system show pitted vessels, often accompanied by fibers and rectangular cells containing clusters and prisms of calcium oxalate. Fragments of spongious parenchyma with large extracellular spaces. Fragments of leaf in transverse view showing a uniform cuticle, underlying pavement cells, and parenchyma. Fragments of straight or slightly curved, multicellular, uniseriate covering trichomes from the base, apex, and adaxial midvein with smooth, thick cell walls. *Buxi folium* diagnostic fragments are depicted in Fig. 3.

The microscopic preparations made from powdered *Arctostaphylos uva-ursi* (L.) Spreng. leaf show fragments of adaxial epidermis in surface view, showing irregular polygonal pavement cells with slightly curved and beaded cell walls, often accompanied by underlying palisade parenchyma. Fragments of abaxial parenchyma in surface view comprised of irregularly polygonal cells with beaded walls often accompanied by underlying spongy parenchyma with large extracellular spaces. Abaxial parenchyma in surface view also shows discrete anomocytic stomata, positioned above extracellular spaces, and covering trichome scars. Fragments of adaxial epidermis in transverse section, showing a uniform cuticle covering pavement cells with beaded walls and underlying elongated 2-4 layers of palisade parenchyma, some containing calcium oxalate crystals. Fragments of the vascular system, consisting of pitted vessels, are often accompanied by rectangular cells containing clusters and prisms of calcium oxalate crystals and fibers with pitted cell walls. Fragments of unicellular covering trichomes, usually curved, with minutely pitted walls. *Uvae ursi folium* microscopic diagnostic characteristics are depicted in Fig. 4.

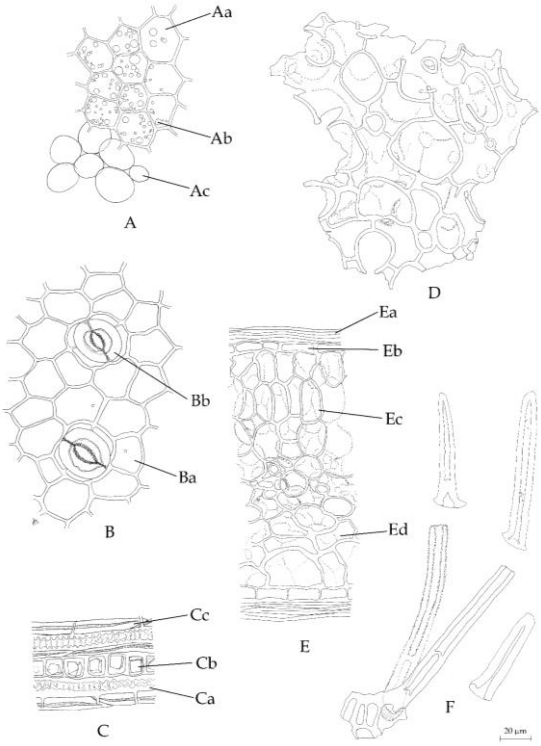

Figure 3. Micromorphological diagnostic characteristics of Boxwood leaf (*Buxi folium*) in bright field.

Fragments of adaxial parenchyma in surface view **(A)**, pavement cells **(Aa)**, spherical oil globules **(Ab),** and palisade parenchyma **(Ac)**. Fragments of abaxial parenchyma in surface view, showing pavement cells **(Ba)** and anomocytic stomata **(Bb)**. Fragments of the vascular system **(C)**, pitted vessels **(Ca)**, rectangular cells with oxalate crystals **(Cb),** and fibers **(Cc)**. Fragments of spongious parenchyma in dorsal view **(D)**. Fragments of leaf in transverse section **(E)**, uniform cuticle **(Ea)**, pavement cells **(Eb)**, palisade parenchyma **(Ec)**, spongious parenchyma **(Ed)**. Fragments of uniseriate covering trichomes **(F)**. 400x magnification. Author: Asen Stoyanov.

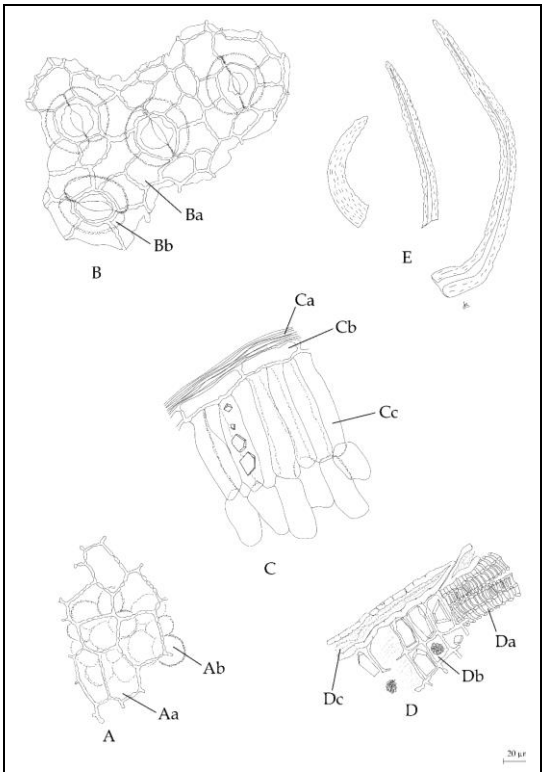

Figure 4. Micromorphological diagnostic characteristics of Bearberry leaf (*Uvae ursi folium*) in bright field.

Fragments of adaxial parenchyma in surface view **(A)**, showing pavement cells **(Aa)** and underlying palisade parenchyma **(Ab)**. Fragments of abaxial epidermis **(B)** in surface view, showing pavement cells **(Ba)** and discreet anomocytic stomata **(Bb)**. Fragments of adaxial epidermis in transverse view **(C)**, showing on opaque cuticle **(Ca)**, underlying epidermal pavement cells **(Cb)** and palisade parenchyma **(Cc)**. Fragments of the vascular system **(D)** comprised of reticulate vessels **(Da)**, rectangular cells containing oxalate crystals **(Db),** and fibers **(Dc)**. 400x magnification. Author: Asen Stoyanov.

Herbal substance micrometry and linear measurements

Microscopic observations showed that the *Arctostaphylos uva-ursi* (L.) Spreng. leaf adaxial epidermis pavement cell wall enclosed the largest area. *Uvae ursi folium* pavement cells appeared larger than those of its adulterant herbal substances under examination. *Arctostaphylos uva-ursi* (L.) Spreng. leaf abaxial epidermis pavement cells were less distinct by comparison. *Uvae ursi folium* had the highest cuticle width, and palisade parenchyma first-layer cells were the longest. Stomatal index values differed significantly for bearberry leaf and box leaf, but not for bearberry leaf and lingonberry leaf. A complete comparison is provided in Table 2.

Teachable machine models

The trained models successfully distinguished *Uvae ursi folium* from its adulterant herbal substances and accurately assigned the highest confidence levels to herbal substance photographic materials. From the models trained on photographic materials of individual diagnostic fragments, the model trained on spongious parenchyma fragments at 25 epochs (100% correct *Uvae ursi folium* classification), but it unsuccessfully identified 1 *Buxi folium* fragment and 2 *Vitis idaeae folium* fragments. Second best was the performance of the model trained on abaxial epidermis-bearing stomata at 25 epochs, which identified 9 of 10 *Uvae ursi folium* fragments and 100% of *Buxi folium* and *Vitis idaeae folium* fragments. All models trained on collages successfully identified 9 of 10 *Uvae ursi folium* fragments but confused 4 of 10 *Buxi folium* fragments with *Vitis idaeae folium*. A complete comparison of the best-performing (most successful identifications) teachable machine models is provided in Table 3. Further comparison of the best-performing models using suitable evaluation metrics after training is provided in Table 4.

Table 2. Comparison of linear measurements and micrometry of diagnostic microscopic characteristics of *Uvae ursi folium*, *Vitis idaeae folium*, and *Buxi folium*.

Microscopic diagnostic characteristic measurement	Herbal substance		
	Uvae ursi folium	***Vitis idaeae folium***	***Buxi folium***
Adaxial epidermis pavement cell area	874.16 ± 24.86[a]	700.41 ± 24.38[b]	475.05 ± 17.02[c]
Adaxial epidermis pavement cell perimeter	116.05 ± 1.78[a]	103.88 ± 2.16[b]	82.70 ± 1.50[c]
Abaxial epidermis pavement cell area	654.37 ± 22.19[a]	509.29 ± 21.36[b]	526.49 ± 20.96[b]
Abaxial epidermis pavement cell perimeter	99.32 ± 1.65[a]	91.38 ± 2,18[b]	89.06 ± 1,89[b]
Adaxial epidermis cuticle width	13.82 ± 0.36[a]	10.30 ± 0.21[b]	9.34 ± 0.29[b]
First layer palisade parenchyma length	64.77 ± 1.06[a]	35.04 ± 0.69[b]	47.33 ± 1.14[c]
Stomatal index	10.04 ± 0.32[a]	9.35 ± 0.35[a]	6.37 ± 0.23[b]

All measurements are in micrometers (µm). Data are expressed as mean ± SEM (n = 50). Treatments not sharing the same letters in the same row are significantly different by ANOVA followed by a Tukey's test ($p<0.05$).

Table 3. Comparison of the teachable machine model's intrinsic parameters and identification of *Uvae ursi folium*, *Vitis idaeae folium*, and *Buxi folium*.

Teachable machine model	Intrinsic parameter						Herbal substance identification					
	Accuracy per class		Accuracy	Test accuracy	Loss	Test Loss	Successful		Semi-successful		Unsuccessful	
Abaxial epidermis bearing stomata, 25 epochs	*Buxi folium*	0.88	1.0000	0.8333	0.0162	0.5122	*Buxi folium*	10	*Buxi folium*	0	*Buxi folium*	0
	Uvae ursi folium	0.75					*Uvae ursi folium*	9	*Uvae ursi folium*	0	*Uvae ursi folium*	1
	Vitis idaeae folium	0.88					*Vitis idaeae folium*	10	*Vitis idaeae folium*	0	*Vitis idaeae folium*	0
Adaxial epidermis in surface view, 10 epochs	*Buxi folium*	1.00	1.0000	0.9583	0.0037	0.1635	*Buxi folium*	9	*Buxi folium*	0	*Buxi folium*	1
	Uvae ursi folium	0.88					*Uvae ursi folium*	8	*Uvae ursi folium*	0	*Uvae ursi folium*	2
	Vitis idaeae folium	1.00					*Vitis idaeae folium*	9	*Vitis idaeae folium*	0	*Vitis idaeae folium*	1
Adaxial epidermis in transverse view, 50 epochs	*Buxi folium*	1.00	1.0000	1.0000	0.0019	0.0645	*Buxi folium*	6	*Buxi folium*	0	*Buxi folium*	4
	Uvae ursi folium	1.00					*Uvae ursi folium*	8	*Uvae ursi folium*	1	*Uvae ursi folium*	1
	Vitis idaeae folium	1.00					*Vitis idaeae folium*	10	*Vitis idaeae folium*	0	*Vitis idaeae folium*	0
Spongious parenchyma, 25 epochs	*Buxi folium*	1.00	1.0000	1.0000	0.0060	0.0303	*Buxi folium*	9	*Buxi folium*	0	*Buxi folium*	1
	Uvae ursi folium	1.00					*Uvae ursi folium*	10	*Uvae ursi folium*	0	*Uvae ursi folium*	0
	Vitis idaeae folium	1.00					*Vitis idaeae folium*	8	*Vitis idaeae folium*	0	*Vitis idaeae folium*	2
Collage, 50 epochs	*Buxi folium*	1.00	1.0000	1.0000	0.0017	0.0356	*Buxi folium*	6	*Buxi folium*	0	*Buxi folium*	4
	Uvae ursi folium	1.00					*Uvae ursi folium*	9	*Uvae ursi folium*	0	*Uvae ursi folium*	1
	Vitis idaeae folium	1.00					*Vitis idaeae folium*	9	*Vitis idaeae folium*	1	*Vitis idaeae folium*	0

Table 4. Comparison of teachable machine model evaluation metrics after model training.

Teachable machine model	Machine learning model evaluation metrics			
	Accuracy	Precision	Selectivity	F1
Abaxial epidermis bearing stomata, 25 epochs	0.97	1.00	0.90	0.95
Adaxial epidermis in surface view, 10 epochs	0.87	0.89	0.80	0.84
Adaxial epidermis in transverse view, 50 epochs	0.82	0.64	0.84	0.73
Spongious parenchyma, 25 epochs	0.90	0.91	1.00	0.95
Collage, 50 epochs	0.82	0.69	0.90	0.78

DISCUSSION

The micromorphological and micrometric exploration of diagnostic characteristics of *Uvae ursi folium* adulterants have, for the first time, elucidated key differences between these herbal substances. Despite notable statistically significant differences in measurements of diagnostic fragments, we caution against basing any conclusion solely on our findings on the identity of herbal substances. As already elaborated, descriptions and linear measurements are contingent on the chosen methodology (Valdecasas, 2023). Furthermore, variability in macroscopic morphological features of herbal substances has been reported for *Arctostaphylos uva-ursi* (L.) Spreng. (Zyber et al., 2017). Additional investigations on the variability of these diagnostic fragments in different plant populations may be warranted. Another consideration is the effect size in the statistically significant differences of diagnostic characteristic measurements as those who differ in wider margins are likely to be easier to notice by an expert observed during sample examination.

In the determination of powdered herbal substance identity, an observer relies on the presence of a combination of specific diagnostic fragments while confirming the absence of others (Ichim et al., 2020). Unfortunately, some of these diagnostic characteristics are lost during primary processing (dehydration), storage and transportation or appear infrequently in microscopic preparations. Such characteristics in *Uvae ursi folium* and its adulterant herbal substances are the covering and glandular trichomes, which are some of their most specific diagnostic fragments. Their rare appearance in these microscopic preparations makes training models based on these structures a less feasible task. Similar considerations should be made in regard to training models on other sets of herbal substances and adulterants. Model training is further hindered by the lack of consideration for different types of photographic materials and image capture devices, which can be used to construct training datasets. While a teachable machine offers the functionality of capturing images via various computer auxiliary hardware devices, such as a built-in web camera (Carney et al., 2020), there is no way to seamlessly select a microscope digital camera as the default photographic material capture device without augmenting the program code.

The optimal model training parameters in plant image recognition for teachable machine are reported as 50 epochs, a batch size of 32, and a learning rate of 0.00001 (Malahina et al., 2024). Our models performed poorly using these values. In order to achieve similar classification success as our current reported findings using a learning rate of 0.00001 and batch size of 32, we needed 250 to 500 epochs, which increases the time required to train models. This suggests that the nature of the photographic materials used to train models has an impact on the optimal values for machine learning model training in teachable machine. Furthermore, during the study design phase, we posited that models trained on more diagnostic characteristics visible in a single image (photographic material collage) would exhibit higher classification success when compared with models trained on single diagnostic fragments. The results of this study could not confirm our hypothesis. However, we deem model evaluation with larger test datasets prudent in this regard.

Several limitations of the current study should be considered when discussing machine learning model performance, namely the relatively small training dataset, the use of only teachable machines for model creation, and the capture of photographic materials in bright field. Training dataset size is a key factor for improving model performance (Gütter et al., 2022), and photographic materials captured in bright-field microscopy are noisy. It is possible that models trained on larger data sets or photographic materials of higher quality would perform better in herbal substance identification. We have not attempted to evaluate the quality of our photographic materials or attempted to improve quality by noise reduction or contrast enhancement post-capture (Cardulo and Hinchcliffe, 2007). Authors have already demonstrated that neural networks perform differently when classifying plant images (Oppong et al., 2022). While teachable machines have a low barrier of entry, other neural networks may perform better in powdered

herbal substance identification. Their capabilities in this regard merit exploration. If computer vision aided microscopy sample authentication is to become routine practice, such hurdles will have to be overcome. In practice, poor performance has been demonstrated by some authors regarding the classification of plants in their native environments (Otter et al., 2021). Other authors have recently reported novel methodologies for macroscopic plant image classification with an accuracy of over 99% (Azadnia et al., 2024), making a strong case for the incorporation of machine learning aided identification. Similar results should be pursued for microscopic plant photographic material classification; however, considering the potential risk of plant and herbal substance misidentification for patients (Cornara et al., 2018), we argue that such tools cannot be used without the oversight of an expert observer.

CONCLUSION

The results of the microscopic examination of *Arctostaphylos uva-ursi* leaf and its adulterants provide critical information for the microscopic detection of foreign matter in powdered samples of herbal substances. The micromorphological study revealed significant qualitative differences in diagnostic tissue fragments, whereas micrometry and linear measurement evaluation elucidated their quantitative differences. Illustrations of herbal substance micromorphology, accompanied by complete descriptions of diagnostic features, were created to facilitate rapid observer microscopic preparation identification. Teachable machine model capabilities for automated microscopic photographic material authentication of powdered herbal substances in bright-field were explored for the first time. The data and results obtained in this study can be used to further refine methodologies for computer vision model training for use in the field of pharmacognostic analysis, identification of herbal substance excipients and constituents, and adulterant screening.

CONFLICT OF INTEREST

The authors declare no conflicts of interest.

ACKNOWLEDGMENTS

The authors thank Prof. Anely Metodieva Nedelcheva, Department of Organic Chemistry and Pharmacognosy at the Faculty of Chemistry and Pharmacy of Sofia University "St. Kliement Ohridski" for confirming botanical identity of collected plant materials. Authors also thank the University Botanical Gardens of Sofia University "St. Kliment Ohridski" for providing *Buxus sempervirens* L. (Buxaceae) leaves. This research was funded by a university project in support of doctoral students – Scientific Research Fund of Sofia University "St. Kliment Ohridski": 80-10-142 / 2024.

REFERENCES

Anh TT, Huy NT, Nhi NTH, Anh TH (2024) Detecting dental caries through captured images using the machine learning technology teachable machine. Asian J Heal Res 3(1): 20–23. https://doi.org/10.55561/ajhr.v3i1.148

Assyov B, Petrova A (2012) Conspectus of the Bulgarian vascular flora. 4th ed., Sofia, Bulgaria: Bulgarian Biodiversity Foundation.

Azadnia R, Noei-Khodabadi F, Moloudzadeh A, Jahanbakhshi A, Omid M (2024) Medicinal and poisonous plants classification from visual characteristics of leaves using computer vision and deep neural networks. Ecol Inform 82: 102683. https://doi.org/10.1016/j.ecoinf.2024.102683

Bokelmann JM (2022) 75 - UVA URSI/Bearberry/Kinnikinic/Bear Grape (*Arctostaphylos uva-ursi*): Leaf. In: Medicinal Herbs in Primary Care, Amsterdam, Netherlands: Elsevier, pp. 645–647. https://doi.org/10.1016/B978-0-323-84676-9.00075-1

Carney M, Webster B, Alvarado I, Phillips K, Howell N, Griffith J, Jongejan J, Pitaru A, Chen A (2020) Teachable Machine: Approachable Web-Based Tool for Exploring Machine Learning Classification. Communication to the CHI '20: CHI Conference on Human Factors in Computing Systems 2020 (Association for Computing Machinery, Honolulu, USA, 25–30 April), pp. 1–8.

Cardullo RA, Hinchcliffe EH (2007) Digital manipulation of brightfield and fluorescence images: Noise reduction, contrast enhancement, and feature extraction. Method Cell Biol 81: 285–314. https://doi.org/10.1016/S0091-679X(06)81014-9

Choudhary M, Sentil S, Jones JB, Paret ML (2023) Non-coding deep learning models for tomato biotic and abiotic stress classification using microscopic images. Front Plant Sci 14: 1292643. https://doi.org/10.3389/fpls.2023.1292643

Cornara L, Smeriglio A, Frigerio J, Labra M, Di Gristina E, Denaro M, Mora E, Trombetta D (2018) The problem of misidentification between edible and poisonous wild plants: Reports from the Mediterranean area. Food Chem Toxicol 119: 112–121. https://doi.org/10.1016/j.fct.2018.04.066

Cybulska P, Thakur SD, Foster BC, Scott IM, Leduc RI, Arnason JT, Dillon JR (2011) Extracts of Canadian first nations medicinal plants, used as natural products, inhibit *Neisseria gonorrhoeae* isolates with different antibiotic resistance profiles. Sex Transm Dis 38(7): 667–671. https://doi.org/10.1097/olq.0b013e31820cb166

Gostin IN (2009) Leaf micromorphology in *Buxus sempervirens* L. during the ontogenesis. Analele Universitatii Din Oradea Fasciculata Biologie XVI: 57–60

Grari M, Yandouzi M, Mohammed B, Boukabous M, Idrissi I (2024) Comparative study of teachable machine for forest fire and smoke detection by drone. Bull Electr Eng Inform 13(3): 1970–1979. https://doi.org/10.11591/eei.v13i3.6578

Guo Y, Kilcrease J, Hammond J, Pooler M (2020) Stomatal openings on boxwood leaves yield entry portals for leaf infection by *Calonectria pseudonaviculata*. J Plant Pathol 102: 213–217. https://doi.org/10.1007/s42161-019-00416-1

Gütter J, Kruspe A, Zhu XX, Niebling J (2022) Impact of training set size on the ability of deep neural networks to deal with omission noise. Front Remote Sens 3: 932431. https://doi.org/10.3389/frsen.2022.932431

Hussein BR, Malik OA, Ong WH, Slik JWF (2022) Applications of computer vision and machine learning techniques for digitized herbarium specimens: A systematic literature

review. Ecol Inform 69: 101641. https://doi.org/10.1016/j.ecoinf.2022.101641

Ichim MC, Häser A, Nick P (2020) Microscopic authentication of commercial herbal products in the globalized market: Potential and limitations. Front Pharmacol 11: 876. https://doi.org/10.3389%2Ffphar.2020.00876

Jovanović A, Drobac M, Vidović B, Pavlović D, Krajnović D, Tadić I (2024) Herbal products versus antibiotics for urinary tract infections-analysis of patient attitudes. J Herb Med 46: 100892. https://doi.org/10.1016/j.hermed.2024.100892

Kavitha S, Kumar TS, Naresh E, Kalmani VH, Bamane KD, Pareek PK (2023) Medicinal plant identification in real-time using deep learning model. SN Comput Sci 5: 73. https://doi.org/10.1007/s42979-023-02398-5

Malahina EAU, Saitakela M, Bulan SJ, Lamabelawa MIJ, Belutowe YS (2024) Teachable machine: Optimization of herbal plant image classification based on epoch value, batch size and learning rate. J Appl Data Sci 5(2): 532–545. https://doi.org/10.47738/jads.v5i2.206

Migas P, Krauze-Baranowska M (2015) The significance of arbutin and its derivatives in therapy and cosmetics. Phytochem Lett 13: 35–40. https://doi.org/10.1016/j.phytol.2015.05.015

Mukherjee PK (2019) Chapter 5 - Morphological and Microscopical Evaluations. In: Quality Control and Evaluation of Herbal Drugs, Amsterdam, Netherlands: Elsevier Inc., pp. 151–193. https://doi.org/10.1016/B978-0-12-813374-3.00005-3

Nedelcheva A, Draganov S (2014) Bulgarian Medical Ethnobotany: The Power of Plants in Pragmatic and Poetic Frames. In: Pieroni A, Quave C (eds.) Ethnobotany and Biocultural Diversities in the Balkans, New York, NY: Springer. https://doi.org/10.1007/978-1-4939-1492-0_4

Oppong SO, Twum F, Hayfron-Acquah JB, Missah YM, Lakshmanna K (2022) A novel computer vision model for medicinal plant identification using log-gabor filters and deep learning algorithms. Comput Intel Nurosc 2022: 1189509. https://doi.org/10.1155/2022/1189509

Otter J, Mayer S, Tomaszewski CA (2021) Swipe right: A comparison of accuracy of plant identification apps for toxic plants. J Med Toxicol 17: 42–47. https://doi.org/10.1007%2Fs13181-020-00803-6

Parate RK, Dhole KM, Sharma SJ (2023) Classification of leaf using teachable machine. Int J Res Appl Sci Eng Technol 11(9): 307–311. https://doi.org/10.22214/ijraset.2023.55629

Powders DMW (2011) Evaluation: from precision, recall and F-measure to ROC, informedness, markedness and correlation. J Mach Learn Technol 2(1): 37–63. https://doi.org/10.48550/arXiv.2010.16061

Radulović N, Blagojević P, Palić R (2010) Comparative study of the leaf volatiles of *Arctostaphylos uva-ursi* (L.) Spreng. and *Vaccinium vitis-idaea* L. (Ericaceae). Molecules 15(9): 6168–6185. https://doi.org/10.3390/molecules15096168

Valdecasas AG (2023) A Cautionary note on linear measurements and their ratios in taxonomy. Taxonomy 3(1): 1–9. https://doi.org/10.3390/taxonomy3010001

Welchman AE (2016) The human brain in depth: How we see in 3D. Annu Rev Vis Sc 2: 345–376. https://doi.org/10.1146/annurev-vision-111815-114605

Wong JJN, Fadzly N (2022) Development of species recognition models using Google teachable machine on shorebirds and waterbirds. J Taibah Univ Sci 16(1): 1096–1111. https://doi.org/10.1080/16583655.2022.2143627

Zyber G, Foto K, Nikollaq B, (2017) The variation of morphological indicators of Uva Ursi (*Arctostaphylos uva-ursi* L.) in Korabi Mountain – Albania. Albanian J Agric Sci 2017 (Special edition): 541–546.

AUTHOR CONTRIBUTION:

Contribution	Stoyanov AS	Gruykin TM	Boyadzhiev MY	Popovski VV
Concepts or ideas	x	x	x	
Design	x	x	x	
Definition of intellectual content	x	x	x	x
Literature search	x		x	x
Experimental studies	x	x	x	x
Data acquisition	x	x	x	x
Data analysis	x	x		x
Statistical analysis	x			
Manuscript preparation	x	x		
Manuscript editing	x			
Manuscript review	x	x	x	x

Citation Format: Stoyanov AS, Gruykin TM, Boyadzhiev MY, Popovski VV (2025) Pharmacognostic analysis and teachable machine automated identification of *Uvae ursi folium*, *Vitis idaeae folium* and *Buxi folium*. J Pharm Pharmacogn Res 13(4): 1191–1201. https://doi.org/10.56499/jppres24.2231_13.4.1191

Publisher's Note: All claims expressed in this article are solely those of the authors and do not necessarily represent those of their affiliated organizations, or those of the publisher, the editors and the reviewers. Any product that may be evaluated in this article, or claim that may be made by its manufacturer, is not guaranteed or endorsed by the publisher.

Open Access: This article is distributed under the terms of the Creative Commons Attribution 4.0 International License (http://creativecommons.org/ licenses/by/4.0/), which permits use, duplication, adaptation, distribution and reproduction in any medium or format, as long as you give appropriate credit to the original author(s) and the source, provide a link to the Creative Commons license and indicate if changes were made.